Weierstraß-Institut
für Angewandte Analysis und Stochastik

im Forschungsverbund Berlin e.V.

Report ISSN 0946 – 8838

Simulation of Pulse Propagation in Nonlinear Optical Fibers

Uwe Bandelow, Ayhan Demircan, Martin Kesting [1]

submitted: 5th May 2003

[1] E-Mail: bandelow@wias-berlin.de, demircan@wias-berlin.de, kesting@wias-berlin.de

No. 23
Berlin 2003

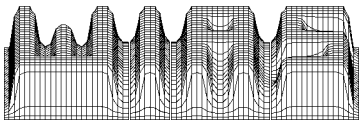

2000 *Mathematics Subject Classification.* 35Q55, 35Q60, 78A60
2003 *Physics and Astronomy Classification Scheme.* 42.65.Tg, 42.81.Dp.

Key words and phrases. Nonlinear Schrödinger Equation, Raman Scattering, Self-Steepening, Solitons, Optical Fiber.

Edited by
Weierstraß-Institut für Angewandte Analysis und Stochastik (WIAS)
Mohrenstraße 39
D — 10117 Berlin
Germany

Fax: + 49 30 2044975
E-Mail: preprint@wias-berlin.de
World Wide Web: http://www.wias-berlin.de/

Abstract

We solve numerically a generalized nonlinear Schrödinger equation by using a pseudospectral method [1]. Integration is performed by using an eight-order Runge-Kutta scheme. The numerical method therefore differs from the commonly used split-step method [2]. Effects such as the impact of group velocity dispersion (GVD) up to fourth-order dispersion, self phase modulation (SPM), self-steepening and intrapulse Raman scattering can be investigated with the code. Examples for the above effects are demonstrated, as well as their interplay in the context of soliton propagation and sub-picosecond pulses.

Contents

1 Introduction

Wave propagation in dispersive nonlinear media has become a topic of intense research activities, in part stimulated by its potential application to optical fiber communication systems. Propagation of optical pulses in monomode optical fibers is mainly influenced by the group velocity dispersion and the refractive index nonlinearity. Rapid progress in ultrashort time laser technology has made it possible that optical pulses with durations comparable to the carrier oscillation cycle can be generated. The propagation of such ultrashort and intense pulses is then affected by additional physical mechanisms, where especially higher order effects become important. Highly nonlinear operating conditions or the interplay between the different linear and nonlinear effects can result in dramatic changes of the temporal and spectral properties of the pulse.

In this paper we want to consider the propagation of pico- and sub-picosecond pulses. The propagation of a sub-picosecond pulse is governed by a generalized nonlinear Schrödinger equation (NLSE), which can be derived from the underlying Maxwell equations within the slowly varying envelope approximation, see Section 2. This means that the pulse envelope $A(z,t)$ modulating the underlying carrier wave $\exp[i(k_0 z - \omega_0 t)]$ is assumed to be slowly varying in time and space. The pulse width has to be much longer than the carrier oscillation period and the spectral content of the field has to be narrower than the carrier frequency ω_0 itself. This is satisfied for optical pulses with widths down to 10fs.

The general form of the NLSE for the complex envelope $A(z,\tau)$ of a pulse is given by

$$\begin{aligned} \frac{\partial A}{\partial z} &= -\frac{i}{2}\beta_2\frac{\partial^2 A}{\partial \tau^2} + \frac{1}{6}\beta_3\frac{\partial^3 A}{\partial \tau^3} + \frac{i}{24}\beta_4\frac{\partial^4 A}{\partial \tau^4} - \frac{1}{2}\alpha A \\ &\quad + i\gamma|A|^2 A - a_1\frac{\partial}{\partial \tau}\left(|A|^2 A\right) - i a_2 A\frac{\partial}{\partial \tau}\left(|A|^2\right) , \end{aligned} \tag{1.1}$$

where the initial value problem

$$A(0,\tau) = f(\tau) \tag{1.2}$$

along z within a retarded time frame $\tau = t - z/v_g$ has to be solved. The linear terms on the right-hand side of Eq.(1.1) are the group velocity dispersion (GVD), namely second-order (SOD), third-order (TOD) and fourth-order dispersion (FOD) and the attenuation term corresponding to the fiber loss α. The main contribution to the group velocity dispersion is represented by the parameter β_2, which leads in general to a broadening of the pulse shape. TOD and FOD are higher order effects arising from the wavelength dependence of the group velocity. These dispersive effects can distort ultrashort optical pulses in the linear as well as in nonlinear regimes. An important fiber parameter is the measure of power loss during the transmission of optical signals inside the fiber, given by the attenuation constant α. The first nonlinear term represents the self-phase modulation (SPM), where $\gamma = n_2\omega_0/cA_{eff}$,

n_2 is the nonlinear refractive-index coefficient, A_{eff} the effective core area and c the speed of light. SPM results from the intensity-dependent refractive index n_2 and is responsible for a large variety of phenomena, such as spectral broadening or optical solitons. The term proportional to a_1 results from the intensity dependence of the group velocity and causes self-steepening and shock formation at the pulse edge with $a_1 = \gamma/\omega_0$. The last term regards the intrapulse Raman scattering and originates from the delayed response, which causes a self-frequency shift. $a_2 = \gamma T_R$, where T_R is related to the slope of the Raman gain. The intrapulse Raman scattering becomes a dominant perturbation for ultrashort pulses and is one of the most important limitations for ultrashort pulse propagation in optical fibers.

In general a numerical approach is needed for an investigation of the generalized NLSE. In this report we want to propose a standard numerical technique, based on a pseudospectral method and a Runge-Kutta scheme, instead of the commonly used split-step method. Our method will be demonstrated for the different physical effects. The examples are chosen such that the results can be compared with analytical and numerical results from the literature.

This report is organized as follows: Section 2 provides the derivation of the generalized nonlinear Schrödinger equation from the Maxwell equations. In Section 3 the used numerical method is discussed and in Section 4 follows a brief description of the usage of the program. Section 5 focuses on the dispersion, which arises from the linear terms under conditions where the nonlinear effects are negligible. Dispersion-induced broadening and higher-order dispersive effects are considered for several pulse shapes. Section 6 is devoted to the nonlinear phenomenon SPM. The features of SPM with and without GVD are discussed. Section 7 is dedicated in particular to the propagation of optical solitons. The impact of the higher order nonlinear terms self-steepening and Raman scattering is subject of Section 8 and 9 respectively.

2 Derivation of the NLSE

The derivation starts from the Maxwell equations for the classical electric and magnetic fields $\mathfrak{E}$, $\mathfrak{H}$

$$\nabla \times \mathfrak{E} + \mu_0 \partial_t \mathfrak{H} = 0 \tag{2.1}$$

$$\nabla \times \mathfrak{H} - \partial_t \mathfrak{D} = \mathrm{j} \tag{2.2}$$

where $\mathfrak{D}$ denotes the electric displacement subject to the linear medium response. The nonlinear (field-dependent) medium response is contained in the current density j and will be treated perturbationally in Section 2.3. The fields $\mathfrak{E}$, $\mathfrak{H}$, $\mathfrak{D}$ and j depend on the three spatial variables $(\mathbf{r})$ and on the time.

The fields propagate longitudinally along the fiber axis which is the z-dimension. The transverse plane is denoted by $\mathbf{r}_t$. The vacuum permeability is denoted by μ_0 and the vacuum permittivity by ε_0. The Fourier transformed quantities are indicated by a tilde.

2.1 Transverse Waveguiding

The fibers under consideration are longitudinally homogeneous, i.e. $\varepsilon = \varepsilon(\mathbf{r}_t)$. Thus, we want to split the Maxwell equations into a stationary transverse system and a longitudinal dynamical system.

We choose a reference frequency ω_0 and seek for a wave number β and solutions $\mathbf{E}$ and $\mathbf{H}$ having the form of a longitudinal wave:

$$\mathbf{E} = \mathbf{e}(\mathbf{r}_t)e^{i(\omega_0 t - \beta z)} \tag{2.3}$$

$$\mathbf{H} = \mathbf{h}(\mathbf{r}_t)e^{i(\omega_0 t - \beta z)}. \tag{2.4}$$

The fields $\mathbf{e}, \mathbf{h}$ solve the transverse waveguide equations

$$\nabla_t \times \mathbf{e}(\mathbf{r}_t) - i\beta \mathfrak{e}_z \times \mathbf{e}(\mathbf{r}_t) + i\omega_0\mu_0\mathbf{h}(\mathbf{r}_t) = 0 \tag{2.5}$$

$$\nabla_t \times \mathbf{h}(\mathbf{r}_t) - i\beta \mathfrak{e}_z \times \mathbf{h}(\mathbf{r}_t) - i\omega_0\varepsilon_0\varepsilon\mathbf{e}(\mathbf{r}_t) = 0. \tag{2.6}$$

Equations (2.5) and (2.6) are restricted to *monochromatic* fields (with optical frequency ω_0) and are independent of z. ∇_t is the transverse component of the nabla operator and $\mathfrak{e}_z := (0,0,1)^T$ the longitudinal unit vector. (2.5), (2.6) is an eigenvalue problem for β and $(\mathbf{e}, \mathbf{h})$ are quadratic in β. It is supposed to contain a discrete spectrum of guided modes. In particular, if $((\mathbf{E}_t, E_z), (\mathbf{H}_t, H_z))$ is an eigenmode with wave number β, $((\mathbf{E}_t, -E_z), (-\mathbf{H}_t, H_z))$ is an eigenmode with wave number $-\beta$. It corresponds to field components propagating in the opposite direction. Motivated by the translational invariance along the fiber we assume no coupling between the counterpropagating fields. Therefore we restrict ourselves to the wave propagating in positive z-direction ($\mathrm{Re}[\beta] > 0$ for positive ω_0).

2.2 Linear Response

We confine ourselves to a single guided transverse mode. This is a good approximation for a *single mode fiber* (SMF), except cases of degenerate modes with different polarization (PMD), which is out of the scope of this paper. The possible excitation of other modes can be taken into account by a phenomenological loss coefficient α later on.

The form of the equations for the mode amplitudes to be derived within this section is independent of the transverse reference mode chosen. Using other types of modes or reference waveguides leads to modified formulas for the coefficients. The only important restriction is, that $\mathfrak{E}$, $\mathfrak{H}$ and j are transversally *single moded*.

The fields are approximated by the following ansatz

$$\mathfrak{E} = \frac{1}{2}A(z,t)\mathbf{e}(\mathbf{r}_t)e^{i(\omega_0 t - \beta z)} + c.c. \tag{2.7}$$

$$\mathfrak{H} = \frac{1}{2}A(z,t)\mathbf{h}(\mathbf{r}_t)e^{i(\omega_0 t - \beta z)} + c.c.. \tag{2.8}$$

Apart from the factor $\exp[i\omega_0 t]$ this ansatz allows the fields to vary in time, which is a non-monochromatic behaviour. According to [3] and [4], the time derivative of the dielectric displacement $\mathfrak{D}$ can then be written as

$$\frac{\partial}{\partial t}\mathfrak{D}(\mathbf{r},t) = \frac{1}{2}e^{i(\omega_0 t-\beta z)}\varepsilon_0 \mathbf{e}(\mathbf{r}_t) i \left(\omega_0\varepsilon(\omega_0) + \frac{\partial \omega\varepsilon(\omega)}{\partial\omega}\Big|_{\omega_0}\left(-i\frac{\partial}{\partial t}\right) + D\right) A(z,t) \quad + c.c., \tag{2.9}$$

where the nonlinear dispersion operator D is defined as

$$D = \sum_{n=2}^{\infty} \frac{1}{n!}\frac{\partial^n \omega\varepsilon(\omega)}{\partial\omega^n}\Big|_{\omega_0}\left(-i\frac{\partial}{\partial t}\right)^n . \tag{2.10}$$

The latter corresponds to an expansion of the *nonlinear dispersion* in the frequency domain as

$$\omega\varepsilon(\omega) = \sum_{n=2}^{\infty} \frac{1}{n!}\frac{\partial^n \omega\varepsilon(\omega)}{\partial\omega^n}\Big|_{\omega_0}(\omega-\omega_0)^n. \tag{2.11}$$

The coefficients $\frac{\partial^n \omega\varepsilon(\omega)}{\partial\omega^n}$ are taken at ω_0 in (2.10) and in (2.11). They may depend on $\mathbf{r}$ but not on the frequency. The result has to be at least a valid approximation for an unperturbated waveguide, where an optical beam with a center frequency ω_0 propagates with the group velocity, rather than the phase velocity.

From now we apply the *Random Phase Approximation* (RPA), i.e. we neglect the "c.c." contributions in (2.7),(2.8) and (2.9). This is a very common approximation which in effect drops fast oscillating terms from the equations.

The Maxwell equations (2.1) and (2.2) read now as

$$\begin{aligned} A\nabla_t \times \mathbf{e} + \partial_z A\mathfrak{e}_z \times \mathbf{e} - A\cdot i\beta\mathfrak{e}_z \times \mathbf{e} + i\omega_0\mu_0 A\mathbf{h} + \partial_t A\mu_0\cdot\mathbf{h} &= 0 && (2.12)\\ A\nabla_t \times \mathbf{h} + \partial_z A\mathfrak{e}_z \times \mathbf{h} - A\cdot i\beta\mathfrak{e}_z \times \mathbf{h} - i\omega_0\varepsilon_0\varepsilon\mathbf{e}A && (2.13)\\ -\varepsilon_0\frac{\partial\omega\varepsilon}{\partial\omega}\mathbf{e}\partial_t A - i\varepsilon_0 D\mathbf{e}A &= 2\mathrm{j}e^{-i(\omega_0 t-\beta z)} \end{aligned}$$

The eigenvalue equations (2.5) and (2.6) for $\mathbf{e}$ and $\mathbf{h}$ provide replacements for the terms $\nabla_t \times \mathbf{e}$ and $\nabla_t \times \mathbf{h}$. The insertion yields

$$\begin{aligned} \partial_z A\mathfrak{e}_z \times \mathbf{e} + \mu_0\cdot\partial_t A\mathbf{h} &= 0 && (2.14)\\ \partial_z A\mathfrak{e}_z \times \mathbf{h} - \varepsilon_0\frac{\partial\omega\varepsilon}{\partial\omega}\partial_t A\mathbf{e} - i\varepsilon_0 D\mathbf{e}A &= 2\mathrm{j}e^{-i(\omega_0 t-\beta z)} && (2.15) \end{aligned}$$

The single mode ansatz is of course to restrictive for satisfying the system (2.14), (2.15) locally. Only a transverse average of (2.14), (2.15) can be satisfied. The averaged equations result from projections, i.e. the scalar products with the modes $\mathbf{h},\mathbf{e}$ respectively, integrated over the transverse plane (denoted by $\int_t d\mathbf{r}_t$).

From the homogeneous waveguide equations (2.5), (2.6) the relations

$$\beta = \omega_0 \frac{\int_t (\varepsilon_0 \varepsilon \mathbf{e}^2 + \mu_0 \mathbf{h}^2)\, d\mathbf{r}_t}{2 \int_t \mathfrak{e}_z \cdot \mathbf{e} \times \mathbf{h} d\mathbf{r}_t}, \tag{2.16}$$

$$\mu_0 \int_t \mathbf{h}^2 d\mathbf{r}_t = \varepsilon_0 \int_t \varepsilon \mathbf{e}^2 d\mathbf{r}_t\,, \tag{2.17}$$

$$\left.\frac{\partial \beta}{\partial \omega}\right|_{\omega_0} = \frac{\varepsilon_0 \int_t (\frac{\partial \omega \varepsilon}{\partial \omega} + \varepsilon) \mathbf{e}^2 d\mathbf{r}_t}{2 \int_t \mathfrak{e}_z \cdot \mathbf{e} \times \mathbf{h} d\mathbf{r}_t} = \frac{k_0^2}{2\beta\omega_0} \cdot \frac{\int_t \left(\varepsilon + \frac{\partial \omega \varepsilon}{\partial \omega}\right) \mathbf{e}^2 d\mathbf{r}_t}{\int_t \mathbf{e}^2 d\mathbf{r}_t} \tag{2.18}$$

($k_0 = \frac{\omega_0}{c}$, TE polarization assumed) can be concluded. The averaged amplitude equation $\int_t d\mathbf{r}_t\, ((2.14) \cdot \mathbf{h} - (2.15) \cdot \mathbf{e})$ becomes:

$$\partial_z A + \partial_t A \cdot \left[\varepsilon_0 \frac{\int_t \left(\varepsilon + \frac{\partial \omega \varepsilon}{\partial \omega}\right) \mathbf{e}^2 d\mathbf{r}_t}{2 \int_t \mathfrak{e}_z \cdot \mathbf{e} \times \mathbf{h} d\mathbf{r}_t} \right] + i \left[\varepsilon_0 \frac{\int_t D \mathbf{e}^2 d\mathbf{r}_t}{2 \int_t \mathfrak{e}_z \cdot \mathbf{e} \times \mathbf{h} d\mathbf{r}_t} \right] A = - \frac{\int_t 2\mathrm{j} e^{-i(\omega_0 t - \beta z)} \cdot \mathbf{e} d\mathbf{r}_t}{2 \int_t \mathfrak{e}_z \cdot \mathbf{e} \times \mathbf{h} d\mathbf{r}_t} \tag{2.19}$$

and will be denoted more shortly as

$$\partial_z A + \frac{\partial \beta}{\partial \omega} \partial_t A + i \sum_{n=2}^{\infty} \frac{\beta_n}{n!} \left(-i \frac{\partial}{\partial t} \right)^n A = -F \tag{2.20}$$

with

$$\beta_n = \varepsilon_0 \frac{\int_t \left. \frac{\partial^n \omega \varepsilon(\omega)}{\partial \omega^n} \right|_{\omega_0} \mathbf{e}^2 d\mathbf{r}_t}{2 \int_t \mathfrak{e}_z \cdot \mathbf{e} \times \mathbf{h} d\mathbf{r}_t} \tag{2.21}$$

and

$$F = \frac{\int_t 2\mathrm{j} e^{-i(\omega_0 t - \beta z)} \cdot \mathbf{e} d\mathbf{r}_t}{2 \int_t \mathfrak{e}_z \cdot \mathbf{e} \times \mathbf{h} d\mathbf{r}_t} = \frac{\mu_0 \omega_0}{2\beta} e^{-i(\omega_0 t - \beta z)} \cdot \frac{\int_t 2\mathrm{j} \mathbf{e} d\mathbf{r}_t}{\int_t \mathbf{e}^2 d\mathbf{r}_t}. \tag{2.22}$$

The coefficients β_n are usually referred to as the group velocity dispersion (GVD) in the literature. For the unidirectional propagation one slows down within a *moving frame*:

$$(z, t) \longmapsto (z, \tau) \quad \text{with} \quad \tau = t - \frac{\partial \beta}{\partial \omega} z \tag{2.23}$$

such that the propagation equation becomes

$$\partial_z A + \frac{\alpha}{2} A + i \sum_{n=2}^{\infty} \frac{\beta_n}{n!} \left(-i \frac{\partial}{\partial \tau} \right)^n A = -F\,. \tag{2.24}$$

In (2.24) the phenomenological fiber loss α has been introduced in addition.

2.3 Nonlinear Response

The response of the fiber is supposed to have a transverse structure proportional to the electric field. We express it in terms of the polarization $\mathbf{P}$:

$$\mathbf{P} = \varepsilon_0 \varepsilon_{NL}(\mathbf{r}_t, z, t) * A(z,t)\mathbf{e}(\mathbf{r}_t)e^{i(\omega_0 t - \beta z)}, \tag{2.25}$$

where $*$ denotes the convolution with respect to time and ε_{NL} is the nonlinear response function [2]

$$\varepsilon_{NL} = \frac{3}{4}\chi^{(3)}\frac{\mathbf{e}^2}{\int \mathbf{e}^2 d\mathbf{r}_t}|A(z,t)|^2. \tag{2.26}$$

We consider only intensity-dependent nonlinear optical effects by (2.26) for shortness [5], [6]. The normalization $\frac{\mathbf{e}^2}{\int \mathbf{e}^2 d\mathbf{r}_t}$ in (2.26) is chosen such that $|A|^2$ becomes the power of the electric field.

The *nonlinear response* (2.26) is often divided into two contributions. One contribution is due to nearly instantaneous (electronic) response and the other is due to delayed (lattice) response (Raman-scattering):

$$\chi^{(3)}(t, t-t_1, t-t_2) = \chi^{(3)}_{xxxx} \cdot [(1-f_R)\delta(t-t_1)\delta(t-t_2) + f_R R(t-t_1)\delta(t-t_2)] \tag{2.27}$$

where R is the Raman response and f_R its relative fraction. Furthermore, the coefficient $\chi^{(3)}_{xxxx}$ is given by

$$\chi^{(3)}_{xxxx} = \frac{8n}{3}n_2 + i\alpha_2\frac{nc}{\omega_0} \tag{2.28}$$

where n is the linear refractive index, n_2 the nonlinear refractive index and α_2 the two-photon absorption coefficient [2].

The current density $\mathrm{j} = \frac{1}{2}(\mathbf{j} + \mathbf{j}^*)$ is the time derivative of the polarization:

$$\mathbf{j} = e^{i(\omega_0 t - \beta z)}\varepsilon_0 \left(i\omega_0 + \frac{\partial}{\partial t}\right)\mathbf{P}(\mathbf{r}_t, z, t), \tag{2.29}$$

such that F in (2.20) becomes

$$\begin{aligned} F &= \frac{k_0^2}{2\beta}\frac{3}{4}\left(\frac{8n}{3}n_2 + i\alpha_2\frac{nc}{\omega_0}\right)\frac{\int \mathbf{e}^4 d\mathbf{r}_t}{\left(\int_t \mathbf{e}^2 d\mathbf{r}_t\right)^2}\left(i + \frac{1}{\omega_0}\frac{\partial}{\partial\tau}\right) \\ &\quad \times \left((1-f_R)|A(z,\tau)|^2 A(z,\tau) + f_R\int_{-\infty}^{\tau} R(\tau-\tau_1)|A(z,\tau_1)|^2 d\tau_1 A(z,\tau)\right) \\ &= \left(\frac{n_2\omega_0}{c} + i\frac{\alpha_2}{2}\right)\frac{\int \mathbf{e}^4 d\mathbf{r}_t}{\left(\int_t \mathbf{e}^2 d\mathbf{r}_t\right)^2}\left(i + \frac{1}{\omega_0}\frac{\partial}{\partial\tau}\right) \\ &\quad \times \left((1-f_R)|A(z,\tau)|^2 A(z,\tau) + f_R\int_{-\infty}^{\tau} R(\tau-\tau_1)|A(z,\tau_1)|^2 d\tau_1 A(z,\tau)\right). \end{aligned} \tag{2.30}$$

For the last step we have used $\beta = nk_0$, such that $\frac{k_0^2}{2\beta} = \frac{\omega_0}{2nc}$. The coefficient

$$A_{eff} = \left(\frac{\int \mathbf{e}^4 d\mathbf{r}_t}{\left(\int_t \mathbf{e}^2 d\mathbf{r}_t \right)^2} \right)^{-1} \tag{2.31}$$

is known as the *effective core area* and often used as a standard fiber parameter in the literature [2], [4]. Using A_{eff} a parameter γ

$$\gamma = \frac{n_2 \omega_0}{c A_{eff}} \tag{2.32}$$

is defined, such that F can be expressed more compactly as

$$\begin{aligned} F &= \left(\gamma + i \frac{\alpha_2}{2A_{eff}} \right) \left(i + \frac{1}{\omega_0} \frac{\partial}{\partial \tau} \right) \\ &\times \left((1 - f_R) |A(z,\tau)|^2 A(z,\tau) + f_R \int_{-\infty}^{\tau} R(\tau - \tau_1) |A(z,\tau_1)|^2 d\tau_1 A(z,\tau) \right). \end{aligned} \tag{2.33}$$

In the following we neglect the two-photon absorption for shortness. Expression (2.33) is still quite general and has been used for studying femtosecond pulses [7]. For pulses longer than 10fs one confines to local approximations of the Raman contribution [2], pp. 47-49. We note

$$\int_{-\infty}^{\tau} R(\tau - \tau_1) |A(\tau_1)|^2 d\tau_1 = \int_0^{\infty} R(\tau') |A(\tau - \tau')|^2 d\tau'. \tag{2.34}$$

Then $|A(\tau - \tau')|^2$ is expanded as:

$$|A(\tau - \tau')|^2 \approx |A(\tau)|^2 - \tau' \frac{\partial}{\partial \tau} |A(\tau)|^2. \tag{2.35}$$

The first moment of the nonlinear response function is used for defining

$$T_R = f_R \int_0^{\infty} \tau' R(\tau') d\tau'. \tag{2.36}$$

Furthermore, we note $\int_0^{\infty} R(\tau') d\tau' = 1$. Inserting this into (2.33) we obtain for Eq.(2.24) the *local equations*

$$\begin{aligned} \frac{\partial}{\partial z} A &= -\frac{\alpha}{2} A - i \sum_{n=2}^{\infty} \frac{\beta_n}{n!} \left(-i \frac{\partial}{\partial \tau} \right)^n A(z,\tau) \\ &\quad -i\gamma \left(1 - \frac{i}{\omega_0} \frac{\partial}{\partial \tau} \right) |A(z,\tau)|^2 A(z,\tau) \\ &\quad +i\gamma T_R \left(1 - \frac{i}{\omega_0} \frac{\partial}{\partial \tau} \right) A(z,\tau) \frac{\partial}{\partial \tau} |A(z,\tau)|^2. \end{aligned} \tag{2.37}$$

The time derivative of the last term is usually neglected in the literature:

$$\begin{aligned}\frac{\partial}{\partial z}A &= -\frac{\alpha}{2}A - i\sum_{n=2}^{\infty}\frac{\beta_n}{n!}\left(-i\frac{\partial}{\partial\tau}\right)^n A(z,\tau) \\ &\quad -i\gamma\left[\left(1-\frac{i}{\omega_0}\frac{\partial}{\partial\tau}\right)|A(z,\tau)|^2A(z,\tau) - T_RA(z,\tau)\frac{\partial}{\partial\tau}|A(z,\tau)|^2\right].\end{aligned} \tag{2.38}$$

In practise, $\sum_{n=2}^{\infty}\frac{\beta_n}{n!}\left(-i\frac{\partial}{\partial\tau}\right)^n A(z,\tau)$ has to be restricted to the first few contributions, expressed by net coefficients β_n which are drawn from measurements. Confining to the lowest terms and taking the complex conjugate of (2.38) one arrives at the generalized *nonlinear Schrödinger Equation* [2]

$$\begin{aligned}\frac{\partial A}{\partial z} &= -\frac{i}{2}\beta_2\frac{\partial^2A}{\partial\tau^2} + \frac{1}{6}\beta_3\frac{\partial^3A}{\partial\tau^3} + \frac{i}{24}\beta_4\frac{\partial^4A}{\partial\tau^4} - \frac{\alpha}{2}A \\ &\quad +i\gamma|A|^2A - \frac{\gamma}{\omega_0}\frac{\partial}{\partial\tau}\left(|A|^2A\right) - i\gamma T_RA\frac{\partial}{\partial\tau}\left(|A|^2\right),\end{aligned} \tag{2.39}$$

which is in the focus of this work. Eq.(2.39) describes the propagation of subpicosecond pulses in optical nonlinear fibers. It is equivalent to Eq.(1.1) with the corresponding coefficients a_1 and a_2.

For the investigations of (2.39) it is sometimes useful to introduce different length scales under which the physical mechanisms can act on the pulse evolution. The crucial physical quantities thereby are the initial pulse width T_0 and the peak power P_0. Depending on these quantities either dispersive or nonlinear effects may dominate the evolution along the fiber. Using these length scales Eq.(2.39) may be transformed in the normalized form:

$$\begin{aligned}i\frac{\partial U}{\partial z} &= \frac{\operatorname{sgn}(\beta_2)}{2L_D}\frac{\partial^2U}{\partial\theta^2} + \frac{i\operatorname{sgn}(\beta_3)}{6L_D'}\frac{\partial^3U}{\partial\theta^3} - \frac{\operatorname{sgn}(\beta_4)}{24L_D''}\frac{\partial^4U}{\partial\theta^4} \\ &\quad -\frac{e^{-\alpha z}}{L_{NL}}\left[|U|^2U + i\frac{1}{\omega_0T_0}\frac{\partial}{\partial\theta}(|U|^2U) + \frac{T_R}{T_0}U\frac{\partial}{\partial\theta}(|U|^2)\right],\end{aligned} \tag{2.40}$$

with the time $\theta = \frac{\tau}{T_0}$ normalized to the initial pulse width T_0. The normalized amplitude is $U(z,\theta) = \frac{1}{\sqrt{P_0}}\exp(\frac{\alpha z}{2})A(z,\theta)$, where P_0 is the peak power of the initial pulse. Specific length parameters are defined as

$$L_D = \frac{T_0^2}{|\beta_2|},\ L_D' = \frac{T_0^3}{|\beta_3|},\ L_D'' = \frac{T_0^4}{|\beta_4|},\ L_{NL} = \frac{1}{\gamma P_0}. \tag{2.41}$$

The second-, third- and fourth-order dispersion lengths L_D, L_D', L_D'' and the nonlinear length L_{NL} provide the length scales over which the different effects become important for pulse evolution along a fiber of length L.

Remarks

1. The neglect of the 2nd derivative with respect to z in the propagation equation (2.39) is no approximation as often claimed in the literature [2].

2. If the pulses become short, their localization in the frequency domain becomes weak. Then especially approximations like (2.27) and the truncation of higher orders of the dispersion become increasingly questionable.

3. An adiabatic invariant of Eq. (2.39) for $\alpha = 0$ is given by [8]:

$$I_1 = \int |A(z,\tau)|^2 \, \mathrm{d}\tau \quad \text{(mass conservation)}. \tag{2.42}$$

4. In the case where $\alpha = 0$ and $a_1 = a_2 = 0$ the NLSE describes a Hamiltonian system. We mention here the momentum and the total energy as the next invariants, cf. [8]:

$$I_2 = \int (A\partial_\tau A^* - A^*\partial_\tau A) \, \mathrm{d}\tau \,,$$

$$I_3 = \int \left(\frac{1}{2}\beta_2 \left|\partial_\tau A\right|^2 - \frac{i}{6}\beta_3(A^*\partial_\tau^3 A - A\partial_\tau^3 A^*) - \frac{1}{12}\beta_4 \left|\partial_\tau^2 A\right|^2 - \gamma \left|A\right|^4\right) \mathrm{d}\tau.$$

3 Numerical Method

The NLSE is a nonlinear partial differential equation which combines nonlinear terms with high-order linear terms and can generally be written in the form

$$\frac{\partial A}{\partial z} = \mathcal{L}A + \mathcal{N}(A) \,. \tag{3.1}$$

Except for some specific cases in which the inverse scattering method or perturbation techniques can be employed, an analytical solution for the generalized NLSE (1.1) is not known. A numerical approach is in general necessary for the evalution of the nonlinear effects. A large number of numerical methods can be used for this purpose. These can be classified into two main categories known as the finite-difference method and the split-step Fourier method. For simulating the NLSE the split-step Fourier method is predominantly used, rather than the finite difference discretization as the split-step Fourier method is often more efficient. In both cases an appropriate discretization of time is needed, leading to a system of ordinary differential equations

$$\frac{\partial \tilde{A}}{\partial z} = \tilde{\mathcal{L}}\tilde{A} + \tilde{\mathcal{N}}(\tilde{A}) \,. \tag{3.2}$$

The split-step method bases on splitting the equation into a linear part

$$\frac{\partial \tilde{A}}{\partial z} = \tilde{\mathcal{L}}\tilde{A} \tag{3.3}$$

and a nonlinear part

$$\frac{\partial \tilde{A}}{\partial z} = \tilde{N}\tilde{A} \tag{3.4}$$

and on solving these equations alternatively. More specifically, it is assumed that the dispersive and the nonlinear effects act independently. In the first step Eq.(3.4) is solved from z to $z + \frac{1}{2}h$ with the initial condition $A(z)$. In the second step the linear equation Eq.(3.3) is solved from $z + \frac{1}{2}h$ to $z + h$ with the solution of Eq.(3.4) as the initial condition for Eq.(3.3). The solution over a short z-interval of length h is then written in the form

$$A(z+h,t) = \exp(\frac{h}{2}\tilde{\mathcal{L}})\exp(\frac{h}{2}\tilde{N})A(z,t)\,.$$

The operators $\tilde{L}$ and $\tilde{N}$ do not commute in general and this propagation from z to $z + h$ is a rough approximation. Based on the Baker-Campbell-Hausdorff formula

$$\exp(\tilde{\mathcal{L}})\exp(\tilde{N}) = \exp\left(\tilde{\mathcal{L}} + \tilde{N} + \frac{1}{2}[\tilde{\mathcal{L}},\tilde{N}] + \frac{1}{12}[\tilde{\mathcal{L}} - \tilde{N},[\tilde{\mathcal{L}},\tilde{N}]] + \cdots\right),$$

a higher-order accuracy can be achieved by applying an appropriate composition of linear and nonlinear steps

$$\begin{aligned} &A(z+h) \approx \\ &\exp(c_1 h\tilde{\mathcal{L}})\exp(d_1 h\tilde{N})\exp(c_2 h\tilde{\mathcal{L}})\exp(d_2 h\tilde{N})\cdots\exp(c_k h\tilde{\mathcal{L}})\exp(d_k h\tilde{N})A(z)\,, \end{aligned} \tag{3.5}$$

where c_i and d_i are real numbers and represent fractional integration steps.

The integration method for the separated parts can in general be performed with different methods, depending on the discretization scheme which has been used. If the influence of boundaries can be ignored, periodic boundary conditions can be imposed with a discretization in the Fourier domain for the time variable. This choice suggests the calculation of the nonlinear part by transforming the amplitude back to the time domain, then to perform the nonlinear operations in the time domain, and finally transforming back to the frequency domain. The solution for the linear part is directly achieved in the frequency domain. Consequently this method is associated to the pseudospectral method. An exact description and an overview of the split-step Fourier method can be found in [2]. The split-step method has the distinction of being a stable integration scheme and has been shown to be convenient because of its simplicity and flexibility in dealing with higher-order dispersion, the Raman effect and filtering [2]. The efficiency depends strongly on the distribution of step-sizes along the fiber. However, for high accuracy a high-order decomposition of $A(z)$ in Eq.(3.5) is needed. But the main advantage lies in the pseudospectral method itself and therewith in the use of the Fast-Fourier transformation (FFT) [9].

In our simulations we will use a different method than the most commonly used for wave propagation in optical fibers. Instead of the split-step Fourier method, we will use a standard dealiased pseudospectral method with a Runge-Kutta integration

scheme [9, 1]. This method calculates also all linear operators and derivatives in the frequency domain and performs the nonlinear multiplications in the time domain, with the transformations between the domains achieved by the Fast Fourier Transformation (FFT). Nonlinear terms need a careful treatment by the spectral method. This is due to the property of the Fourier transformation which states that products in the time domain give rise to convolutions in the frequency domain. Direct evaluation of the convolution sums needs $O(N^2)$ operations. The use of FFT decreases the number of operations down to $O(N \log_2 N)$.

Integration along z is performed in the same step for the linear and the nonlinear part of the equation. We use a variable Runge-Kutta scheme of order three, five or eight with stepsize control depending on the accuracy as described in [10].

It is well-known that in the numerical investigations of systems of differential equations stiffness can occur. The presence of higher-order derivatives in $\mathcal{L}$ implies higher powers of frequencies in $\tilde{L}$. Already at moderately large values of the frequencies $\tilde{L}$ will dominate $\tilde{N}$ and dictate a very small integration step. This stiffness becomes worse as the degree of the highest derivative increases. Therefore we have limited our investigations at present to fourth-order time-derivatives.

In order to solve Eq.(1.1) we impose periodic boundary conditions with a period T in the time domain and express $A(z,\tau)$ in terms of Fourier series as follows:

$$A(z,\tau) = \sum_{n=-\infty}^{\infty} \tilde{A}_n(z) \mathrm{e}^{i\omega_n \tau} \quad \text{with} \quad \omega_n = n\frac{2\pi}{T}\,, \quad n = 0, 1, 2, \ldots \tag{3.6}$$

where n is the integer mode number. With the abbreviations

$$\Psi = |A|^2 A\,, \qquad \Phi = \frac{\partial}{\partial \tau}\left(|A|^2 A\right)\,, \qquad \Xi = A\frac{\partial}{\partial \tau}\left(|A|^2\right)\,, \tag{3.7}$$

for the nonlinearities, which have Fourier expansions like A, we arrive at the analogous of Eq.(1.1) in the frequency domain:

$$\begin{aligned} \frac{\partial \tilde{A}_n(z)}{\partial z} &= \frac{i}{2}\beta_2 \omega_n^2 \tilde{A}_n(z) - \frac{i}{6}\beta_3 \omega_n^3 \tilde{A}_n(z) + \frac{i}{24}\beta_4 \omega_n^4 \tilde{A}_n(z) - \frac{\alpha}{2}\tilde{A}_n(z) \\ &\quad + i\gamma \tilde{\Psi}_n(z) + a_1 \tilde{\Phi}_n(z) - i a_2 \tilde{\Xi}_n(z)\,, \end{aligned} \tag{3.8}$$

with

$$\begin{aligned} \tilde{\Psi}_n(z) &= \sum_{l-m+k=n} \tilde{A}_l(z) \tilde{A}_m^*(z) \tilde{A}_k(z) \\ \tilde{\Phi}_n(z) &= i\omega_n \sum_{l-m+k=n} \tilde{A}_l(z) \tilde{A}_m^*(z) \tilde{A}_k(z) \\ \tilde{\Xi}_n(z) &= i \sum_{l+m=n} \tilde{A}_l(z) \omega_m \sum_{k-q=m} \tilde{A}_k(z) \tilde{A}_q^*(z)\,. \end{aligned}$$

These nonlinear terms are evaluated in the time domain and the overall convolution sequence used in this code can be summarized by

$$\tilde{A}_n,\, i\omega\tilde{A}_n \stackrel{\text{IFFT}}{\longrightarrow} A,\, \partial_\tau A \stackrel{\times}{\longrightarrow} |A|^2 A = \Psi,\, A\partial_\tau |A|^2 = \Phi \stackrel{\text{FFT}}{\longrightarrow} \tilde{\Psi}_n,\, \tilde{\Phi}_n,\, \tilde{\tilde{\Xi}}_n\,,$$

where IFFT means the Inverse Fourier Transformation, $\times$ is the multiplication in the time domain and FFT means the Fourier Transformation back into the frequency domain. However, the use of this method can lead to an alias error [1] due to the use of a truncated Fourier series, as we will show now. The calculation of a convolution sum

$$\tilde{C}_n = \sum_{p+q=n} \tilde{A}_p \tilde{B}_q \tag{3.9}$$

by a pseudospectral method leads to

$$\begin{aligned} \tilde{C}_n &= \frac{1}{N}\sum_{j=0}^{N-1} A_j B_j e^{-i\omega_n \tau_j} \\ &= \frac{1}{N}\sum_{j=0}^{N-1} \sum_{|p|\le N/2} \tilde{A}_p e^{i\omega_p\tau_j} \sum_{|q|\le N/2} \tilde{B}_q e^{i\omega_q\tau_j}\, e^{-i\omega_n\tau_j} \\ &= \sum_{|p|,|q|\le N/2} \tilde{A}_p\tilde{B}_q \frac{1}{N}\sum_{j=0}^{N-1} e^{i(\omega_p+\omega_q-\omega_n)\tau_j}\,. \end{aligned} \tag{3.10}$$

Using the orthogonality relation for the discrete Fourier transformation

$$\sum_{j=0}^{N-1} e^{-i(\omega_n-\omega_p)\tau} = \begin{cases} N \text{ if } n = p(\text{mod } N) \\ 0 \end{cases},$$

equation (3.10) can be written as

$$\tilde{C}_n = \sum_{p+q=n} \tilde{A}_p\tilde{B}_q + \sum_{p+q=n\mp N} \tilde{A}_p\tilde{B}_q\,. \tag{3.11}$$

The second term on the right-hand side in (3.11) is the alias error which can been seen by comparing it with Eq.(3.9). It originates from the property that $e^{i(\omega_n+\omega_N)\tau_j} = e^{i\omega_n\tau_j}$ for all integer j, n such that the discrete grid points τ_j cannot distinguish the frequency ω_n and its alias $\omega_{n+N}, \omega_{n\mp 2N}$, etc.. For any $n < N/2$, there always exists a nonzero aliasing error. Therefore our simulation needs a dealiasing method [1].

A further possible error which can occur in spectral methods is the Gibbs phenomen. It occurs with a truncated or a discrete Fourier series in the neighborhood of a point of discontinuity. The partial sums of a Fourier series exhibit a substantial overshoot near these points and oscillations indicate this phenomenon. If our simulations contain derivatives which are to steep for the simulation grid to be resolved, the solution will exhibit discontinuities. This can be circumvented in our simulations by applying a higher resolution, see Sec. 4.

4 Usage of the Program

The resolution of the simulation is expressed by the number of modes nt over which the convolution term is computed and has to be a power of 2 for FFT convenience. The number nt has to be specified by the user in the file `resolution.for`. When appropriate, dealising is performed using the two-thirds rule [1]. With the dealised procedure the amplitude is constructed in the time domain using only modes with numbers between $-ndt/2$ and $ndt/2$. So the user might specify ndt in `resolution.for` minding the condition $0 < ndt \leq \frac{2}{3}nt$. Without dealiasing ndt has to be equal to nt. After setting the resolution the program has to be compiled with `'f90 main.f -o nlse -r8'`, where `nlse` is the name chosen for the executable code.

The data for a specific problem have to be provided in the file `para.dat`. The different parameters and the names for the output files have to be specified according to the structure given in Tab.(1). Changes in `para.dat` do not require to recompile the program.

The initial values for $A(z_0, \tau)$ can be provided by the user in a separate file `start.vec`. In this case $in = 0$ has to be set. Alternatively ($in = 1$) the initial values will be generated according to the following parameters:

- $m = 0$ chirped Hyperbolic-Secant Pulse:
  $A(z_0, \tau) = A_0 \,\mathrm{sech}\left(\frac{\tau}{T_0}\right) \exp\left(-\frac{iC\tau^2}{2T_0^2}\right)$
- $m \neq 0$ chirped Super-Gaussian Pulse
  $A(z_0, \tau) = A_0 \exp\left(-\frac{1+iC}{2}\left(\frac{\tau}{T_0}\right)^{2m}\right)$.

In both cases the file `start.vec` stores the initial values $\tilde{A}(\omega_n) := \tilde{A}_n(z_0)$. According to the resolution ndt the real and imaginary parts $\tilde{A}_R(\omega_n)$, $\tilde{A}_I(\omega_n)$ of $\tilde{A}(\omega_n)$ for $-ndt/2 \leq \omega_n \leq ndt/2$ will be stored in a one-dimensional array $Y(\mathrm{i})$ of length $dimf := 2(ndt + 1)$. The convention is $Y(\mathrm{i}) = \tilde{A}_R(-ndt/2 + (\mathrm{i} - 1)/2)$ for i = 1, 3, ..., $dimf - 1$ and $Y(\mathrm{i}) = \tilde{A}_I(-ndt/2 + (\mathrm{i} - 2)/2)$ for i = 2, 4, ..., $dimf$. Hence, `start.vec` contains simply the vector $Y(\mathrm{i})$, i = 1, ..., $dimf$ providing initial values in the frequency domain.

The integration along z is then performed in the frequency domain for the real array $Y(\mathrm{i})$. Output is generated for the initial condition at z_0 and after every distance z_{out}.

type	example	parameter	description
real*8	1.0d1	T	time period (for FFT)
real*8	1.0d0	β_2	SOD coefficient
real*8	0.1d0	β_3	TOD coefficient
real*8	0.01d0	β_4	FOD coefficient
real*8	1.0d0	γ	SPM coefficient
real*8	0.01d0	a_1	self-steepening coefficient
real*8	0.01d0	a_2	Raman-scattering coefficient
real*8	0.1d0	α	fiber loss coefficient
real*8	1.0d0	$A_0 = \sqrt{P_0}$	amplitude of the initial pulse
real*8	1.0d0	T_0	width of the initial pulse
real*8	0.0d0	z_0	initial z-value
real*8	1.0d0	z_{end}	final z-value
real*8	1.0d0	z_{out}	distance for generation of output
integer	$0\|1$	in	initial value: 0 – read, 1 – generate
integer	$0\|1\|2,\ldots$	m	pulse: 0 – sech, $1, 2, \ldots$ – Super-Gauss
integer	$0\|-1\|1,\ldots$	C	chirp: 0 – non, $\pm1, \pm2, \ldots$ chirped
character*40	'start.vec'	file	start vector Y(i)
character*40	'vector.int'	file	vector after the integration
character*40	'moden.int'	file	selected integrated modes
character*40	'energ.int'	file	norm and broadening factor
integer	1	n_1	mode numbers of spectral component
integer	3	n_2	which will be observed during
integer	7	n_3	the integration in the file `moden.int`
integer	9	n_4	

Table 1: Structure of `para.dat` and exemplary values

The states $\tilde{A}_n(z)$, $A(z)$ for $z = z_0$+j$*z_{out}$, j = 0, 1, ... (depending on the distance z_{out} and the length of the interval $[z_0, z_{end}]$) are saved in files `z_**.omg` and `z_**.time` respectively, where `**` corresponds to the value of j. These files have the following structure (the columns are separated by white space):

`z_**.omg`: The first item is the value of z followed by four columns. The first column contains values of $\omega_n := \mathrm{i} * 2\pi/T$, where the integer $\mathrm{i} = -ndt/2, \ldots, ndt/2$. The subsequent columns store the associated values of $\tilde{A}(\omega_n) := \tilde{A}_n(z)$ in the form $|\tilde{A}(\omega_n)|^2$, $\tilde{A}_R(\omega_n)$, $\tilde{A}_I(\omega_n)$ respectively.

`z_**.time`: The first item is the value of z followed by four columns. The first column contains values of τ running from $-T/2$ to $T/2$ in steps of size $T/(nt-1)$. The subsequent columns store the associated values of $|A(z,\tau)|^2$, $A_R(z,\tau)$, $A_I(z,\tau)$ respectively.

The final state $\tilde{A}_n(z_{end})$ is stored in a file `vector.int` analogous to `start.vec`, using the same structure of the vector $Y(\mathrm{i})$ as described above. So it might be directly used for further integration by regarding it as `start.vec`.

`moden.int` contains the z-evolution of the four spectral components, which are specified in `para.dat` by n_1, n_2, n_3, n_4.

`energ.int` contains the z-evolution of adiabatic invariants $\int |A(z,\tau)|^2 d\tau$, $\int |\tilde{A}(z,\omega)|^2 d\omega$ and of the *broadening factor* σ/σ_0 defined by the variance

$$\sigma = (< \tau^2 > - < \tau >^2)^{1/2} , \tag{4.1}$$

where the n-th moment $< \tau^n >$ is given by

$$< \tau^n >= \frac{\int \tau^n |A(z,\tau)|^2 d\tau}{\int |A(z,\tau)|^2 d\tau} .$$

The invariants can be used for checking the correctness of the calculation in the following sense: If in the case $\alpha = 0$ (no fiber loss) the invariants are not preserved, it is most likely that a numerical instability occurs. A common possible error is an inadequate value for the time period T. This will be explained in the following sections. Another possibility is the requirement of a higher resolution or more precise values for the error tolerance. The error tolerance has to be changed directly in `main.f` and requires recompilation of the program.

5 Group Velocity Dispersion

As long as the nonlinear effects play a minor role, the dispersive effects govern the pulse propagation. This is the case for fiber lengths $L \approx L_D \ll L_{NL}$. For standard telecommunication fibers the parameters at $\lambda = 1.55\mu$m are $\beta_2 \approx 20\text{ps}^2/\text{km}$ and $\gamma \approx 3\text{W}^{-1}\text{km}^{-1}$. So, $L_D \ll L_{NL}$ is satisfied, for example, in the case $T_0 \sim 1$ps and $P_0 \ll 1$W. In order to investigate the dispersive effects alone, we deal with the fourth-order *linear* Schrödinger equation

$$\frac{\partial A}{\partial z} = -\frac{i}{2}\beta_2 \frac{\partial^2 A}{\partial \tau^2} + \frac{1}{6}\beta_3 \frac{\partial^3 A}{\partial \tau^3} + \frac{i}{24}\beta_4 \frac{\partial^4 A}{\partial \tau^4} \tag{5.1}$$

throughout this section. In general, the main effect of dispersion is to broaden an optical pulse as it propagates through the fiber. The solutions of Eq.(5.1) scale with the dispersion lengths defined in (2.41). Therefore we will not give explicit units for T_0, β_i and P_0 in the following examples, except they are explicitly mentioned.

5.1 Second-Order Dispersion (SOD)

To study the effects of SOD alone β_3 and β_4 are set to zero in Eq.(5.1). The β_2-term represents the dispersion of the group velocity and varies with the wavelength. For longer wavelengths it becomes negative (anomalous dispersion) and vanishes at the zero-dispersion wavelength λ_D. SOD changes the phase of each *spectral component* of the pulse by an amount that depends on the frequency and the propagated distance.

For an unchirped Gaussian pulse ($C = 0$) the induced broadening does not depend on the sign of β_2, see Fig. 1 left. The pulse width increases during the propagation. Short pulses broaden more rapidly because of their smaller dispersion length ($L_D \sim |T_0|^2$).

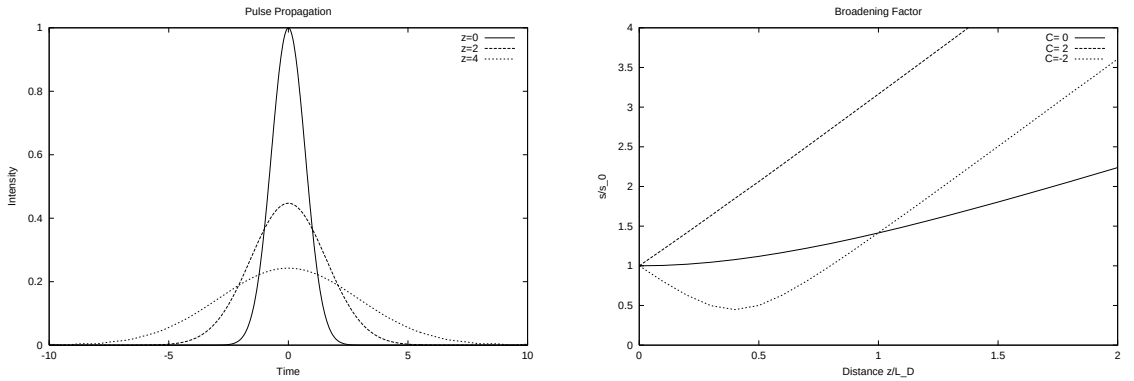

Figure 1: *Left: unchirped Gaussian pulse at $z = 0$, $z = 2L_D$ and $z = 4L_D$ for $\beta_2 = \pm 1$, $T_0 = 1$, $P_0 = 1$, $T = 20$, $nt = 512$, (cf. [2] Fig. 3.1). Right: Variation of broadening factor σ/σ_0 with propagated distance for different Gaussian pulses with $C = -2; 0; 2$ where $\beta_2 > 0$, (cf. [2] Fig. 3.2).*

For chirped pulses one observes a different effect. If the sign of the chirp-factor C is the opposite of the sign of β_2, the pulse initially narrows (and therefore becomes higher), because the dispersion-induced chirp is in opposite direction to the initial chirp. The broadening starts when the induced chirp dominates. Conversely, if the chirp-factor and β_2 possess the same sign the broadening takes place at a higher rate than for an unchirped pulse, see Fig. 1 right. The importance of the adequate period

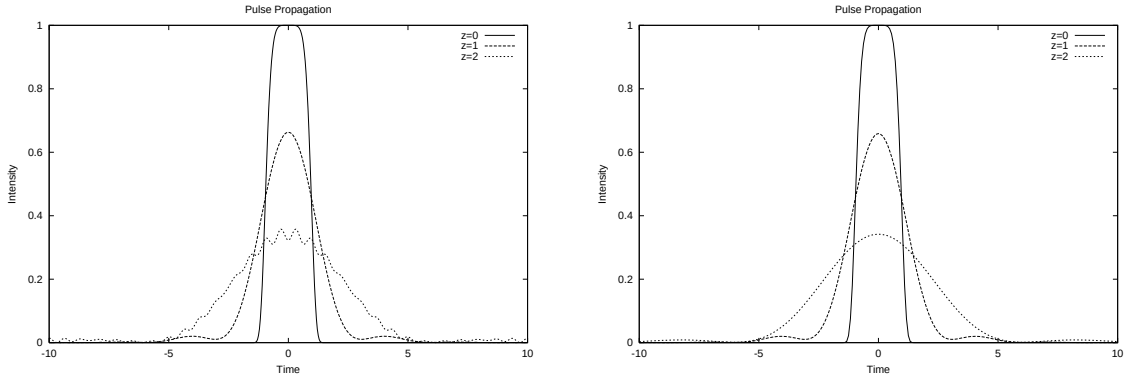

Figure 2: *Unchirped Super-Gaussian pulse ($m = 3$) at $z = 0$, $z = L_D$ and $z = 2L_D$. Left: $T = 20$, (cf. [11], Fig. 3.4) – oscillations are due to numerical instabilities. Right: $T = 40$ (cf. [2], Fig. 3.4) – no oscillations occur.*

T for the simulation can be demonstrated by the following example, see Fig. 2. We consider an unchirped Super-Gaussian pulse with $C = 0$, $m = 3$, $T_0 = 1$, $P_0 = 1$, where $\beta_2 = 1$ and $T = 20; 40$, $nt = 512$ are used for the simulation. The oscillations

of the pulse shape in the case $T = 20$ are due to numerical instabilities caused by the small time period. The fast broadening of the pulse leads to such effects as the pulse energy reaches the boundary of the time window.

5.2 Third-Order Dispersion (TOD)

If the pulse wavelength lies in the vicinity of the zero-dispersion wavelength λ_D ($\beta_2 \approx 0$), the β_3-term provides the dominant contribution to the dispersive effects. Also for ultrashort pulses (widths $T_0 < 1$ps) the contribution of TOD can not be neglected, because the expansion parameter $\Delta\omega/\omega_0$ is no longer small enough to justify a truncation of the expansion. In general, the TOD effects play a significant role if $L_D^{'} \leq L_D$.

We consider the following example (Fig. 3) left: Unchirped Gaussian pulse with $T_0 = 1$, $P_0 = 1$, where $\beta_3 = 1$. The TOD-effect alone ($\beta_2 = 0$) is compared with the situation, where $L_D = L_D'$, that is, if $\beta_2 = 1$.

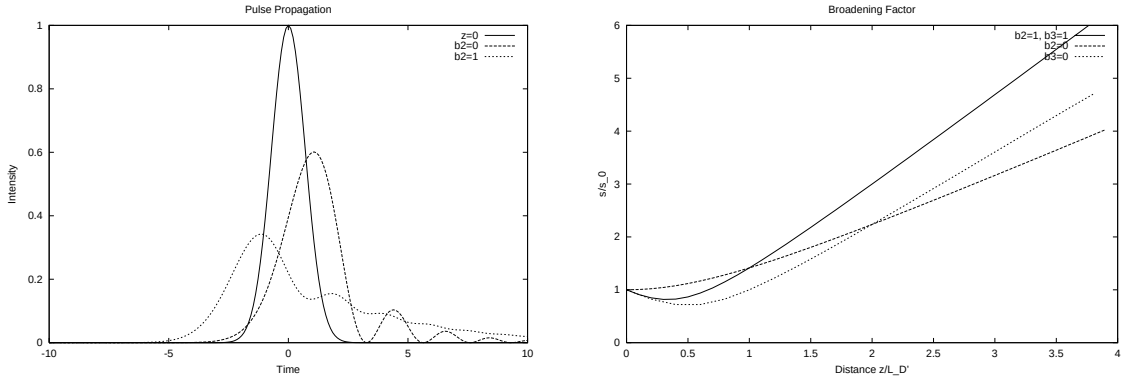

Figure 3: *Left: unchirped Gaussian pulse for $\beta_3 = 1$, $\beta_2 = 0; 1$ at $z = 0$, $z = 5L_D'$, (cf. [2] Fig. 3.6). Right: broadening factor σ/σ_0 along the propagated distance for a chirped Gaussian pulse ($C = -1$) where $\beta_2 = 0; 1$, $\beta_3 = 0; 1$.*

The pulse is distorted such that it becomes asymmetric with an oscillatory structure near of its edges. These oscillations are damped significantly if SOD is present, as in the case $L_D = L_D'$.

The interplay between SOD and TOD may also be illustrated by the impact on the broadening factor σ/σ_0. We consider the evolution of a chirped Gaussian pulse ($C = -1$) for $\beta_2 = 1$, $\beta_3 = 1$ and compare it with the situations, where $\beta_2 = 0$ or. $\beta_3 = 0$ at the same scale ($L_D' = 1$ or $L_D = 1$), see Fig. 3 right. In cooperation SOD and TOD produce the highest broadening rate. In the case of $\beta_2 = 0$ (at the zero-dispersion wavelength), the chirped pulse is not initially narrowed, which means TOD alone does not cause this effect in contrast to SOD. Furthermore, the broadening rate of TOD alone is smaller than the one of SOD in the case of chirped pulses.

5.3 Fourth-Order Dispersion (FOD)

For ultrashort pulses (widths $T_0 \approx 10$fs), the β_4-contribution is expected to be of influence because spectral widths of potentially more than 1000THz have to be covered. Qualitatively, the fourth-order effects are quite similar to the SOD effects. The impact of FOD becomes important if L_D'' is near L_D or even beneath as in the case of ultrashort pulses (keep in mind $L_D'' \sim |T_0|^4$).

If β_2 and β_4 have the same sign, the dispersion effect is qualitatively the same as in the case of SOD alone. Therefore we first examine the following example: Propagation of an unchirped Gaussian pulse with $T_0 = 1$, $P_0 = 1$, where $\beta_2 = -1$, $\beta_3 = 0$, $\beta_4 = +1$. In this case the dispersion lengths are $L_D = L_D''$, $L_D' = \infty$. The propagated pulse is shown in Fig. 4 left at $z/L_D = 0; 3; 6; 9$. In the calculations $T = 200$, $nt = 1024$ have been used.

Dispersion takes place by spreading the energy of the pulse symmetrically, but the contribution of β_4 is to generate oscillations aside the center of the pulse. This results principally from the different signs of β_2 and β_4. Depending on the ratio of L_D and L_D'' this effect will be more or less important. That means, if SOD dominates, the oscillation due to FOD will be spread out quickly as well.

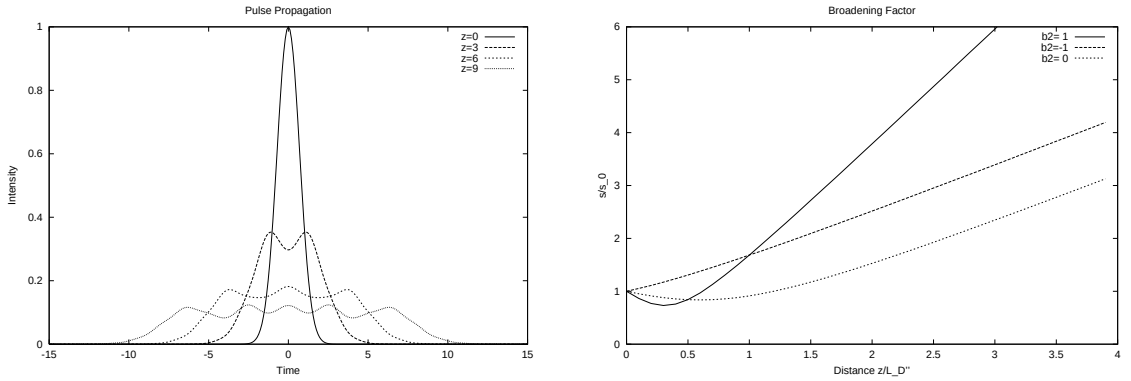

Figure 4: *Left: unchirped Gaussian pulse,* $\beta_2 = -1$, $\beta_4 = +1$ *at* $z/L_D'' = 0; 3; 6; 9$. *Right: broadening factor* σ/σ_0 *along the propagated distance for a chirped Gaussian pulse* $(C = -1)$ *where* $\beta_4 = 1$, $\beta_2 = \pm 1$ *or* $\beta_2 = 0$.

The influence of β_4 in cooperation with β_2 on the broadening factor is shown in Fig. 4 right for a chirped Gaussian pulse $(C = -1)$ with $T_0 = 1$, $P_0 = 1$ where $\beta_2 = \pm 1; 0$, $\beta_3 = 0$, $\beta_4 = +1$. The effect of FOD at the zero-dispersion length on a chirped pulse is similar to those of SOD alone, but weaker (cf. also Fig. 3 right). In the case of $L_D = L_D''$ the β_2-term dominates such that its sign determines the qualitative behavior of the broadening factor at the beginning.

The interplay between TOD and FOD at the zero-dispersion length is shown in an example quite similar to the one before, see Fig. 5 left. The parameters are as follows: Chirped Gaussian pulse $(C = -1)$ with $T_0 = 1$, $P_0 = 1$ where $\beta_2 = 0$, $\beta_3 = 0; 1$, $\beta_4 = 0; 1$. So it is $L_D' = 1$ or $L_D'' = 1$, to which the propagated distance is

related. Again, FOD alone has a weaker effect than the lower order term TOD, but in cooperation they cause a higher broadening rate.

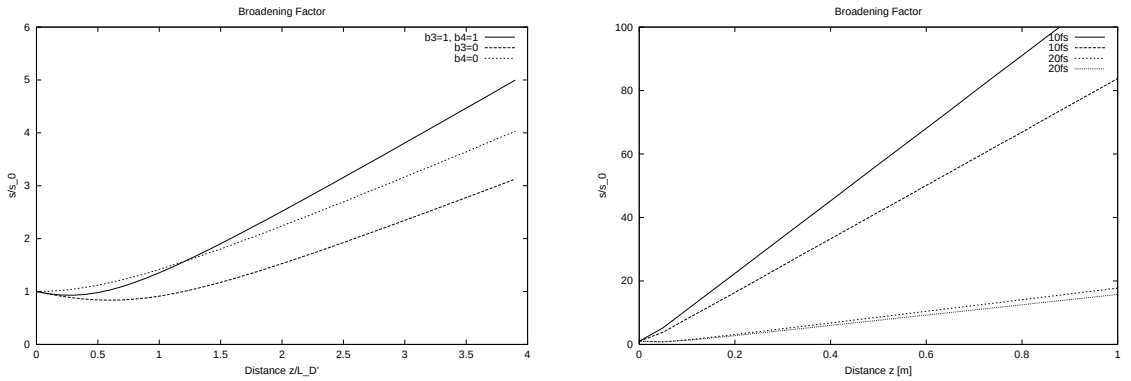

Figure 5: *Broadening factor σ/σ_0 along the propagated distance for a chirped Gaussian pulse ($C = -1$). Left: $T_0 = 1$, $P_0 = 1$, where $\beta_2 = 0$, $\beta_3 = 0; 1$, $\beta_4 = 0; 1$. Right: specific parameters given within the text, upper curve used $\beta_4 = 4.91 \times 10^{-7}\mathrm{ps}^4/\mathrm{m}$, lower curve used $\beta_4 = 0$ for* 10fs- *or* 20fs-*pulse.*

Finally we consider an example with the specific values $\beta_2 = 4.08 \times 10^{-3}\mathrm{ps}^2/\mathrm{m}$, $\beta_3 = 6.13 \times 10^{-5}\mathrm{ps}^3/\mathrm{m}$, $\beta_4 = 4.91 \times 10^{-7}\mathrm{ps}^4/\mathrm{m}$, taken from [12]. The first two values are measured at the fiber used in the experiments, but β_4 is fitted to the data according to the numerical model used there. The impact of the higher order terms on the broadening factor will be shown in the case of ultrashort pulses $T_0 = 10$ and $T_0 = 20\mathrm{fs}$, but note that the nonlinear terms are still neglected. We do this just to demonstrate the importance of taking FOD into account, bearing in mind that the real evolution of such pulses will strongly depend on the nonlinearities. Clearly, the described propagation takes place near the zero-dispersion length. For a 10fs pulse the dispersion lengths are $L_D = 0.245\mathrm{m}$, $L'_D = 0.163\mathrm{m}$, $L''_D = 0.204\mathrm{m}$. So it should be sufficient to look at the evolution of the broadening factor up to $z = 1\mathrm{m}$, see Fig. 5 right. We used a chirped Gaussian pulse ($C = -1$) and the parameters $T = 50\mathrm{ps}$, $nt = 8192$ for the simulation. The upper curves for $T_0 = 10\mathrm{fs}$ and $T_0 = 20\mathrm{fs}$ represent the calculations with the given parameters. The second curves beneath belong to the simulations with $\beta_4 = 0$, all other parameters as before. It is to be seen, that for the 20fs-pulse the difference is still small, but for the 10fs-pulse a conspicuous effect occurs. Hence, it is worth to consider the third- and fourth-order dispersion in the model.

6 Self-Phase Modulation (SPM)

Now we step back to the NLSE (1.1), but with $a_1 = a_2 = 0$ throughout this and the next section. In particular nonlinear effects governed by γ come into play. The corresponding length scale L_{NL} is independent of the dispersion length L_D. L_D depends on the pulse width and L_{NL} on the peak power (cf. Eq.(2.41)). If the fiber

length is such that $L \approx L_{NL}$ but $L \ll L_D$ the nonlinear effect of SPM dominates. Typical values would be for example $T_0 > 100$ps with a large peak power $P_0 \geq 1$W and $\gamma = 20\mathrm{W}^{-1}\mathrm{km}^{-1}$. Self-Phase Modulation is defined as the change of an optical pulse due to the self-induced change in the nonlinear refractive index. A temporal varying phase $\phi(\tau)$ of $A(z,\tau)$ is connected to a frequency generation:

$$\delta\omega(\tau) = \frac{\partial\phi(\tau)}{\partial\tau}\,.$$

This implies that the instantaneous optical frequency $\omega(\tau) = \omega_0 + \delta\omega(\tau)$ differs across the pulse from its central value ω_0. Pure SPM induces intensity- and time-dependent phase shifts and a chirp which magnitude increases with z. New frequency components are continuously generated, which yields a broadening of the spectrum. The latter is illustrated by the following example (Fig. 6):

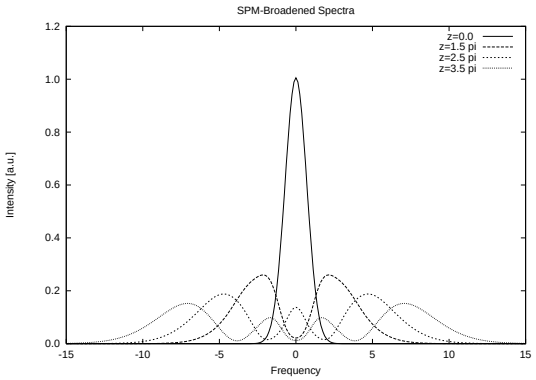

Figure 6: *Calculated SPM-broadened spectra for an unchirped Gaussian pulse* $T_0 = 1$, $P_0 = 1$, $\gamma = 1$ *and* $\beta_n = 0$ *(cf. [2], Fig. 4.2).*

The excitation of higher frequency components leads to multipeak spectra with the outermost peaks becoming the most intense. The SPM-broadened spectrum depends on the pulse shape and on the initial chirp. Fig. 7 left compares the pulse spectra for Gaussian and Super-Gaussian ($m = 3$) pulses. In the calculation used for Fig. 7 the fiber length and peak power are chosen such that both spectra exhibit 5 peaks. The spectral range for the Super-Gaussian pulse is about three times larger with most of the energy at the central peak. An initial frequency chirp leads also to a change in the pulse spectrum. This is illustrated in Fig. 7 right which shows the spectra of a Gaussian pulse with positive and negative chirp ($C = 5$ and $C = -5$) under the same conditions as in Fig. 6. A positive chirp increases the number of spectral peaks while the opposite occurs in the case of a negative chirp.

The combination of the SPM-term with the dispersion terms (β_n) leads to new qualitative features. The most prominent is the support of soliton propagation through the fiber which is subject to the next section exclusively.
It is useful to introduce the scaling

$$N^2 = \frac{L_D}{L_{NL}} = \frac{\gamma P_0 T_0^2}{|\beta_2|}, \tag{6.1}$$

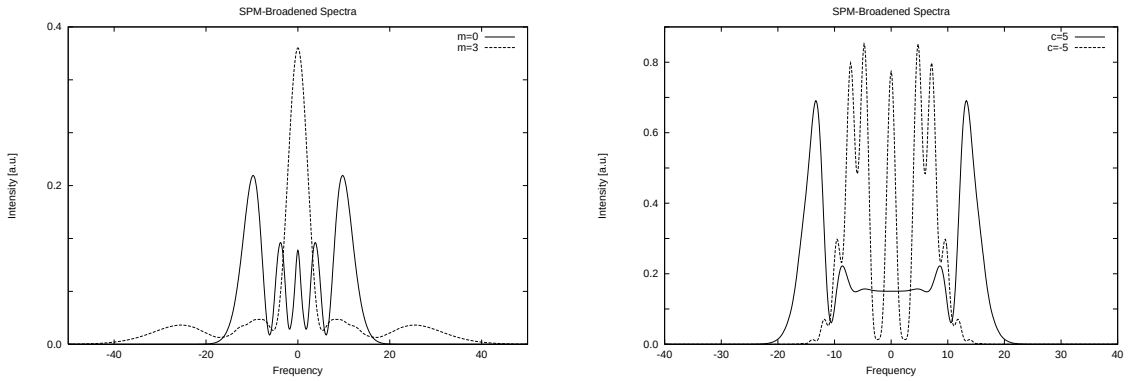

Figure 7: *Left: Comparison of SPM-broadened spectra for unchirped Gaussian (solid) and super-Gaussian (dashed) pulses at a peak power corresponding to* $z = 4.5\pi L_D$ *(cf. [2], Fig. 4.4); Right: Effect of initial chirp on SPM-broadened spectra of a chirped Gaussian pulse with* $C = 5$ *and* $C = -5$ *(*$z = 4.5\pi L_D$*) (cf. [2], Fig. 4.5).*

where N measures the relative importance of the SOD and the SPM effects. The integer values of N are related to the soliton order [2]. Different combinations can lead to the same N. If $N = 1$ for example as $T_0 = 1$ps and $P_0 = 1$W, the calculated results apply equally to $T_0 = 10$ps and $P_0 = 10$mW or $T_0 = 0.1$ps and $P_0 = 100$W.

The impact of SOD on SPM is illustrated by two examples for $N = 1$.
The first example (Fig. 8) is for normal dispersion ($\beta_2 = 1$, $\gamma = 1$):

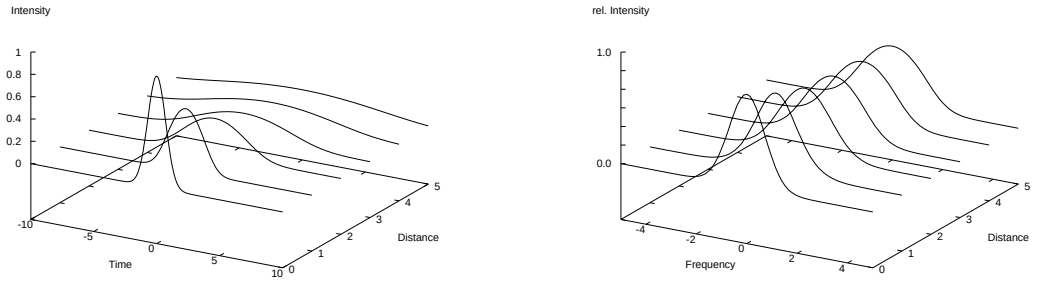

Figure 8: *Evolution of the pulse shape (left) and pulse spectrum (right) over a distance* $z = 5L_D$ *for an initially unchirped Gaussian pulse propagating in the normal-dispersion regime of the fiber (*$\beta_2 > 0$*) and* $N = 1$ *(cf. [2], Fig. 4.7).*

The pulse broadens much more rapidly compared to the case without GVD. In the absence of GVD a two-peak spectrum is reached at $z = 5L_D$.

The second example (Fig. 9) considers anomalous dispersion ($\beta_2 = -1$, $\gamma = 1$):

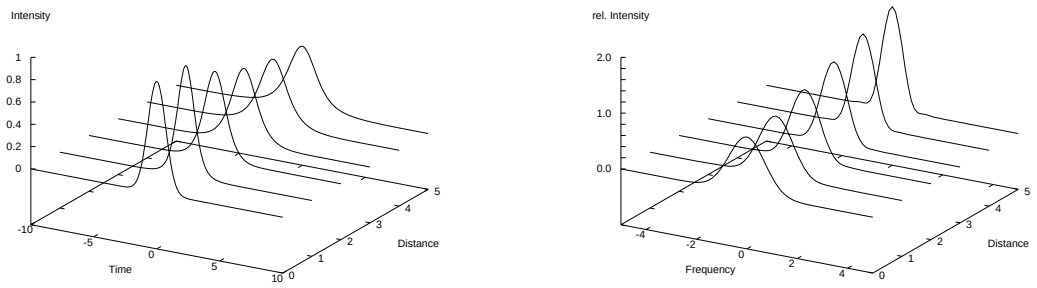

Figure 9: *Evolution of the pulse shape (left) and of the pulse spectrum (right) over a distance $z = 5L_D$ for an initially unchirped Gaussian pulse propagating in the anomalous dispersion regime of the fiber ($\beta_2 < 0$) with parameters such that $N = 1$ (cf. [2], Fig. 4.8) .*

The pulse broadens initially at a rate much lower than expected in the absence of SPM and it approaches a steady state for $z > 4L_D$. The spectrum narrows due to the fact that the SPM-induced chirp is positive while the dispersion-induced chirp is negative. The SOD and SPM cooperate with each other to maintain a chirp-free pulse and shape the pulse in such a way that it appears to converge to a hyperbolic-secant pulse.

In conclusion, SPM enhances the broadening rate in the normal-dispersion regime and decreases it in the anomalous dispersion regime. Furthermore, even weak dispersive effects can lead to significant pulse shaping. This will be illustrated by another example (Fig. 10) where SPM dominates ($N = 30$).

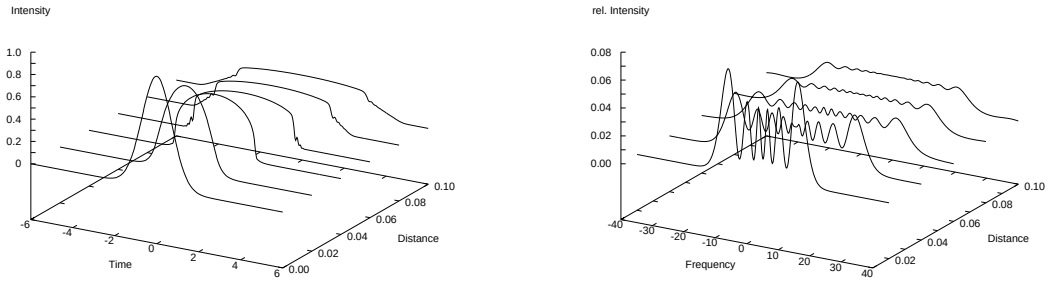

Figure 10: *Evolution of the pulse shape (left) and of the pulse spectrum (right) over a distance $z/L_D = 0.1$ for an initially unchirped Gaussian pulse propagating in the normal-dispersion regime of the fiber ($\beta_2 > 0$) with parameters such that $N = 30$ (cf. [2], Fig. 4.10 and Fig. 4.11).*

The pulse becomes nearly rectangular accompanied by a linear chirp. The effectiveness of SOD becomes large near the pulse edges (large curvature). An oscillatory structure near the pulse edge can be observed at about $z/L_D = 0.06$, which is

termed as *optical wave breaking*. The latter results from *four-wave-mixing* effects, which excite higher frequencies in turn by the nonlinear interaction. Different parts of the pulse propagate at different speeds. A positive initial chirp would increase the SPM-induced chirp and optical wave breaking would set in earlier.

It turns out that even if the SPM dominates ($N \gg 1$) the SOD cannot be treated as a perturbation. This is due to the large amount of the induced frequency chirp imposed by SPM on the pulse which affects SOD, see Section 5. No optical wave breaking occurs in the case of anomalous SOD ($\beta_2 < 0$).

Also the TOD can influence pulse shapes and spectra significantly. For the examination of pulse propagation at the zero-dispersion wavelength ($\beta_2 = 0$) we define another scaling parameter

$$N'^2 = \frac{L_D'}{L_{NL}} = \frac{\gamma P_0 T_0^3}{|\beta_3|}, \tag{6.2}$$

which measures the relative importance of TOD and SPM.
The next example (Fig. 11) considers the case $N' = 1$ and $\beta_2 = 0$:

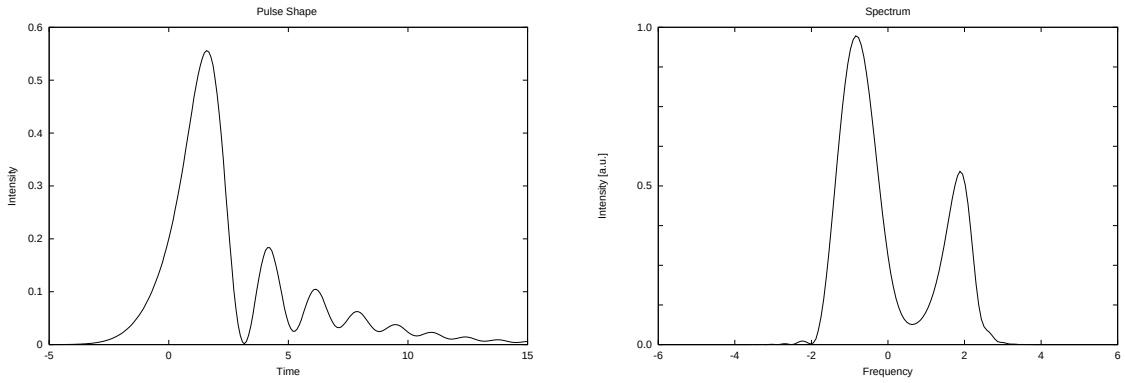

Figure 11: *Shape (left) and spectrum (right) of an initially unchirped Gaussian pulse which propagates exactly at the zero-dispersion wavelength, such that* $\beta_2 = 0$, $\beta_3 > 0$, $N' = 1$ *and* $z = 5L_D'$ *(cf. [2], Fig. 4.14).*

The shape of the pulse shown in Fig. 11 left exhibits oscillations. The appearance of these oscillations are caused by TOD, see Section 5. However, the intensity does not become zero at the oscillation minima, which is due to the interplay with SPM. As can be seen in Fig. 11 right the TOD introduces a spectral asymmetry. In the absence of TOD a symmetric two-peak spectrum would be expected. The impact of the interplay of TOD and SPM on the spectrum is different from the interplay of SOD and SPM in the normal dispersion case, where SOD hinders the splitting of the spectrum.

7 Soliton Propagation

In optical fiber communication solitons are potentially very attractive, because they maintain their shape and their spectrum during the propagation. However, fibers can support solitons only in the anomalous-dispersion regime ($\beta_2 < 0$). Moreover, they are disturbed by further effects as absorption, higher order dispersion, Raman scattering, self-steepening and more. The latter two effects play an important role for pulses shorter than 1ps and will be investigated in the next sections. Throughout this section we will confine to SPM, losses and dispersion effects.

We consider initial value problems for solitons with the following initial condition:

$$A(0,\tau) = N\,\mathrm{sech}(\tau) \tag{7.1}$$

where N is the soliton order defined by Eq.(6.1). Another important quantity in this context is the soliton period z_s defined by (cf. [4])

$$z_s = \frac{\pi}{2} L_D = \frac{\pi}{2} \frac{T_0^2}{|\beta_2|}. \tag{7.2}$$

We begin with the fundamental soliton for $N = 1$. More specifically, we start with the loss-free case $\alpha = 0$ and chose $\beta_2 = -1$, $\gamma = 1$, $\beta_3 = 0$, $\beta_4 = 0$, see Fig. 12. In

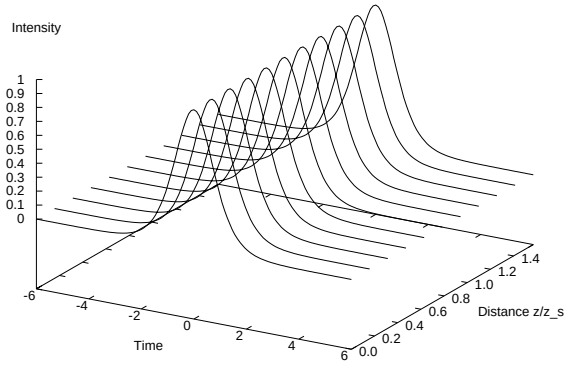

Figure 12: *Fundamental Soliton propagation over one soliton period in a nonlinear lossless optical fiber.*

this case, the dispersion length L_D is equal to the nonlinear length L_{NL}, $N^2 = 1$. The normalized equation Eq.(2.40) with $\xi = z/L_D$ takes the form of the standard nonlinear Schrödinger equation

$$i\frac{\partial U}{\partial \xi} + \frac{1}{2}\frac{\partial^2 U}{\partial \theta^2} + |U|^2 U = 0\,, \tag{7.3}$$

with the fundamental soliton solution $U(\xi,\theta) = \mathrm{sech}(\theta)\exp(i\xi/2)$. For such a first-order soliton SOD and SPM balance each other, that neither the pulse shape nor the spectrum changes along the fiber length.

Now we take the fiber loss ($\alpha > 0$) into account. The resulting pulse shapes are shown in Fig. 13. The pulse amplitude decreases gradually due to the fiber loss. For the lower loss the pulse width increases significantly. In effect, the nonlinearity is no longer strong enough to compensate the SOD effect, hence SOD increasingly takes over. For the higher loss the soliton pulse amplitude decreases more rapidly and the signal vanishes before a significant broadening can take place.

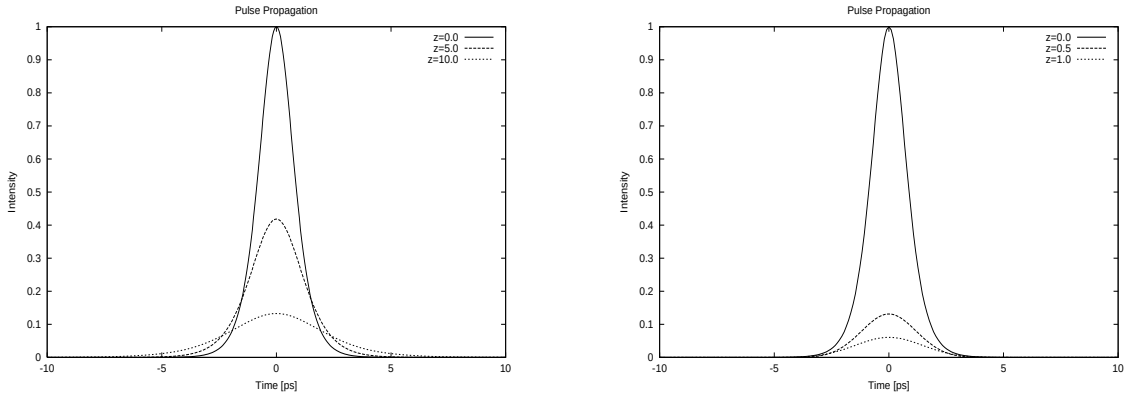

Figure 13: *Fundamental soliton propagation over 10 soliton periods in a conventional optical fiber. Left:* $\alpha = 0.074$, *Right:* $\alpha = 0.74$ *(cf. [13] Fig. 3 and Fig. 5).*

To point out the periodicity of soliton solutions we consider the propagation of a third-order soliton: $N = 3$, $\beta_2 = -1$, $\gamma = 9$, $\beta_3 = \beta_4 = 0$, which is drawn in Fig. 14.

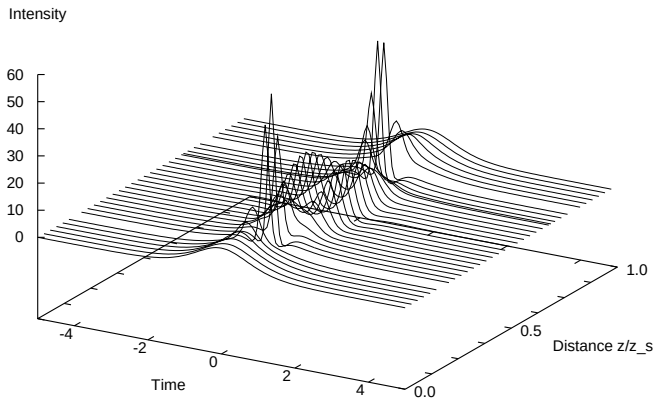

Figure 14: *Temporal evolution over one soliton period for the third-order soliton. Note pulse splitting near* $z/z_s = 0.5$ *and soliton recovery beyond that (cf. [2], Fig. 5.4).*

We observe a periodic evolution for higher-order solitons. As the pulse propagates along the fiber it first contracts to a fraction of its initial width, splits afterwards

into two distinct pulses at the half period length and then merges again to recover the original shape at the end of the soliton period. The spectrum is also periodic, as to be seen in Fig. 15.

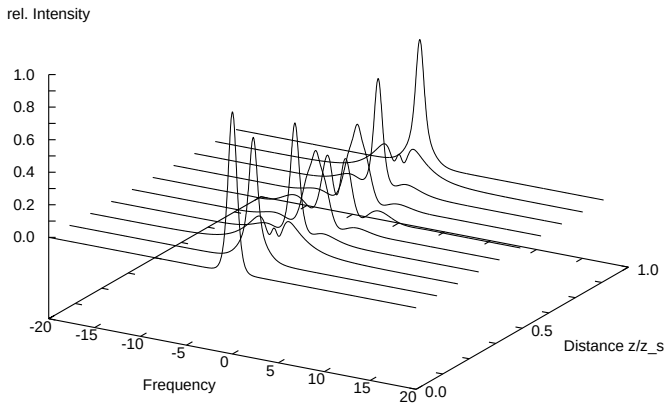

Figure 15: *Spectral evolution over one soliton period for the third-order soliton in Fig. 14 (cf. [2], Fig. 5.5).*

In conclusion, solitons survive by a balance between SPM and SOD. The SPM generates a frequency chirp and induces spectral broadening. SOD contracts the pulse if the pulse is positively chirped. For higher-order solitons SPM dominates initially but SOD leads then to a contraction. Higher order dispersion is expected to shape the spectrum asymmetrically, as discussed in Section 5.2, thereby destroying the periodic behaviour of solitons.

8 Self-Steepening

In this section we will consider the impact of the nonlinear term governed by $a_1 = \frac{1}{\omega_0 T_0}$ on the standard nonlinear Schrödinger equation, which can cause self-steepening in particular. Self-steepening results from the intensity dependence of the group velocity. It affects ultrashort pulses of width $T_0 < 100$fs. We consider first the dispersionless case ($\beta_2 = \beta_3 = \beta_4 = 0$) using the parameters $\gamma = 1$ and $a_1 = 0.01$, shown in Fig. 16. As can be seen there, an optical shock is created on the trailing edge of the pulse. Dispersion would dissipate the shock in effect, cf. [11]. Self-steepening also induces a time-shift of the pulse center which is due to the intensity-dependent change of the group velocity.

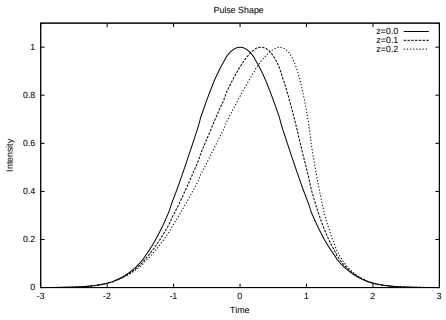

Figure 16: *Self-steepening of a Gaussian pulse in the dispersionless case (cf. [2], Fig. 4.16)* .

For higher-order solitons the self-steepening is breaking the degeneracy of the solitons, leading to a break-up into their constituents (soliton decay), such that the constituents propagate at different speed. We illustrate this by another example for a second-order soliton $\beta_2 = -1$, $\gamma = 1$, $\beta_3 = 0$, $N = 2$, $a_1 = 0.2$, drawn in Fig. 17.

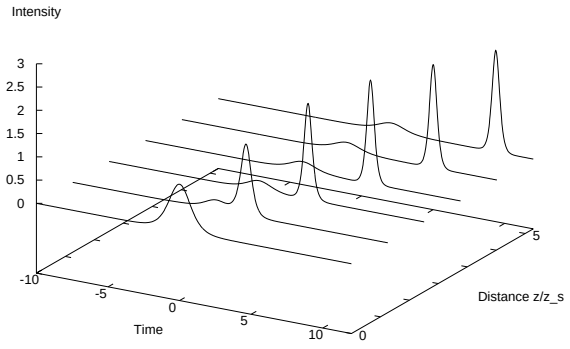

Figure 17: *Decay of a second-order soliton* ($N = 2$) *induced by self-steepening* ($a_1 = 0.2$). *Pulse evolution over five soliton periods is shown (cf. [2], Fig. 5.17).*

9 Intrapulse Raman Scattering

Now we will study the impact of a_2 on the standard nonlinear Schrödinger equation, which is known as the intrapulse Raman scattering. In difference to the self-steepening, Raman scattering comes from the delayed lattice response. Raman scattering causes self-frequency shifts for pulse widths $T_0 \approx 1$ps and shorter. The Raman scattering amplifies the low-frequency spectral components with high-frequency components acting as a pump. The energy is continuously transferred from the blue components to red components, so that it appears as a red shift of the soliton spectrum, which increases with the distance.

See, for example, Fig. 18 which is for the parameters $\beta_2 = -1$, $\gamma = 1$, $\beta_3 = 0$, $N = 2$, $a_2 = -0.01$. At a first glance Fig. 18 seems to be similar to Fig. 17. However

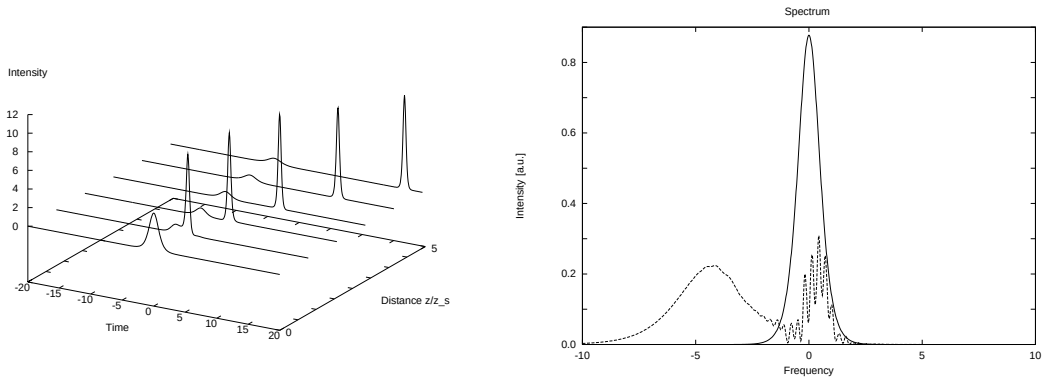

Figure 18: *Left: Decay of a second-order soliton* ($N = 2$) *induced by intrapulse Raman scattering* ($a_2 = -0.01$) *(cf. [2], Fig. 5.18). Right: Pulse spectrum at* $z = 0$ *(solid) and* $z/z_s = 5$ *(dashed) (cf. [2], Fig. 5.19).*

there is a difference in the shift of the two pulses. In the case of intrapulse Raman scattering the low-intensity pulse is advanced, whereas the high-intensity pulse is not. In the case of self-steepening both pulses are delayed, cf. Fig. 17.

Mathematically, the Raman contribution (governed by a_2) reduces the symmetry of the propagation equation (1.1), such that invariants are lost. Consequently, there exists no soliton solution for the full equation (1.1). Moreover, no Lagrangian can be found for that case [8].

10 Conclusion

We have demonstrated a numerical method for the simulation of pulse propagation in nonlinear optical fibers. By using a pseudospectral scheme the code solves a generalized nonlinear Schrödinger equation. A non-standard derivation of this nonlinear Schrödinger equation from the Maxwell equations has been given in this report. The numerical solution of this equation was performed by using an eight-order Runge-Kutta scheme with step-size control, which is more precise than the widely applied split-step fourier method. Details of the numerical method and its implementation have been described as well as the practical usage of the code.
Demonstrating the code different effects of importance for the propagation of optical pulses in nonlinear fibers have been studied. In particular, the impact of group velocity dispersion up to fourth-order dispersion, self phase modulation and their interplay has been investigatet. As the most prominent application of this interplay the propagation of optical solitons has been studied in more detail. Moreover, perturbations caused by self-steepening and intrapulse Raman scattering can be investigated with the code, which has been demonstrated by several examples.

A Code Description

The code is written in FORTRAN90 and is structured as follows. The main program, which has to be compiled as described in Sec. 4, uses several subroutines which are contained in separate files. We describe in the following table the input data and the generated output for every subroutine.

routine `file`	used subroutines	description
NLSE `main.f`	INITIALIZE, DOP853, SOLOUT	the main program, compiled as described in Sec. 4
INITIALIZE `main.f`	FFT	generates the initial pulse $A(0,\tau)$ as $Y(\mathrm{i})$ input: `para.dat, start.vec`, output: `start.time, start.omg`
DOP853 `dop853.f`	FCN, SOLOUT	explicit Runge-Kutta scheme of order 8(5,3) with stepsize control for a system of non-stiff first order ordinary differential equations, code is described in [10]
SOLOUT `main.f`	FD, TD	writes out the numerical solution during and at the end of the integration, input: $Y(\mathrm{i}), z_0, z_{end}, z_{out}$, output: `*.int, *.omg, *.time` as described in Sec. 4
FCN `rhs.f`	FT	calculates the right-hand side $F(\mathrm{i})$ of Eq. (3.8), the nonlinear terms are calculated as products in the time domain input: $Y(\mathrm{i})$, output: $F(\mathrm{i})$
FD `fd.f`	–	input: $Y(\mathrm{i})$, output: $\|\tilde{A}_n\|$, $\|\tilde{A}_n\|_{\max}$, $\omega(\|\tilde{A}_n\|_{\max})$
FT `ft.f`	FFT	Fourier-Transformation of the discretely sampled data $A(z,\tau)$ or $\tilde{A}_n(z)$, processes the normalization and storage arrangements for the specific FFT used, input/output: $A(z,\tau)$, $\tilde{A}_n$
FFT `fft.f`	–	standard FFT-routine as described in [9]
TD `td.f`	FT	transformes $F(\mathrm{i})$ into the time domain, input: $Y(\mathrm{i})$, output: $A_{\max}$, $\tau(A_{\max})$, $\|A\|$, $\|A(z,\tau)\|$, σ/σ_0

References

[1] C. Canuto, M. Y. Hussaini, A. Quarteroni, and T. A. Zang. *Spectral Methods in Fluid Dynamics*. Springer, Berlin, 1988.

[2] G. P. Agrawal. *Nonlinear Fiber Optics*. Optics and Photonics. Academic Press, 3rd edition, 2001.

[3] L. D. Landau and E. M. Lifschitz. *Electrodynamics of Continuous Media*, volume 8 of *Course of Theoretical Physics*. Pergamon Press, London, 1960.

[4] A. Hasegawa. *Optical Solitons in Fibers*. Springer, 1989.

[5] R. W. Boyd. *Nonlinear Optics*. Academic Press, San Diego.

[6] Y. R. Shen. *The Principles of Nonlinear Optics*. Wiley, 1984.

[7] A. L. Gaeta. Nonlinear propagation and continuum generation in microstrucutred optical fibers. *Optics Letters*, 27(11):924–926, June 2002.

[8] V. I. Karpman. Radiation of solitons described by a high-order cubic nonlinear Schrödinger equation. *Physical Review E*, 2000.

[9] W. H. Press, B. P. Flannery, S. A. Teukolsky, and W. T. Vetterling. *Numerical Recipes, The Art of Scientific Computing, FORTRAN Version*. Cambridge University Press, Cambridge, England, 1989.

[10] E. Hairer, S. P. Nørsett, and G. Wanner. *Solving Ordinary Differential Equations I*. Springer, Berlin, 1993.

[11] G. P. Agrawal. *Nonlinear Fiber Optics*. Optics and Photonics. Academic Press, 2nd edition, 1995.

[12] G. Boyer. High-power femtosecond-pulse reshaping near the zero-dispersion wavelength of an optical fiber. *Optics Letters*, 24(14):945–947, July 1999.

[13] Shum P. Ghafouri-Shiraz H. and Nagata M. A novel method for analysis of soliton propagation in optical fibers. *IEEE Journal of quantum electronics*, 31(1):190–200, January 1995.